

1 **Recent Southwestern U.S. drought influenced by anthropogenic**
2 **aerosols and tropical ocean warming**

3 Yan-Ning Kuo¹, Flavio Lehner^{1,2,3}, Isla R. Simpson², Clara Deser², Adam S. Phillips²,
4 Matthew Newman⁴, Sang-Ik Shin^{4,5}, Spencer Wong⁶, Julie Arblaster⁶

5 *¹Department of Earth and Atmospheric Sciences, Cornell University, Ithaca, NY, USA*

6 *²Climate and Global Dynamics Laboratory, NSF National Center for Atmospheric*
7 *Research, Boulder, CO, USA*

8 *³Polar Bears International, Bozeman, MT, USA*

9 *⁴Physical Sciences Laboratory, National Oceanic and Atmospheric Administration,*
10 *Boulder, CO, USA*

11 *⁵CIRES, University of Colorado, Boulder, CO, USA*

12 *⁶School of Earth Atmosphere and Environment, Monash University, Melbourne, VIC,*
13 *Australia*

14

15 **Abstract**

16 The Southwestern U.S. (SWUS) is currently in a multi-decade drought that has developed
17 since the 1980s. While anthropogenic warming has made the drought more severe, it is
18 the decline in winter-spring precipitation that has had a more profound effect on water
19 resources and ecosystems. This precipitation decline is not well understood beyond its
20 attribution to the post-1980 La Niña-like cooling trend in tropical sea surface temperatures
21 (SSTs), which caused a North Pacific anticyclonic atmospheric circulation trend
22 conducive to SWUS precipitation declines. Using a hierarchy of model simulations, we
23 show that, even under El Niño-like SST trends, there is a tendency towards a North Pacific
24 anticyclonic circulation trend and SWUS precipitation declines, counter to the canonical
25 El Niño teleconnection. This unintuitive yet robust circulation change arises from non-
26 additive responses to tropical mean warming and radiative effects from anthropogenic
27 aerosols. As the forced SWUS precipitation decline combines with anthropogenic
28 warming, the post-1980 period shows the fastest SWUS soil moisture drying among past
29 and future periods of similar length. While the precipitation trend might reverse due to
30 future projected El Niño-like warming and aerosol emission reduction, it is unlikely to
31 alleviate the currently projected future drought risk.

32

33 **Main**

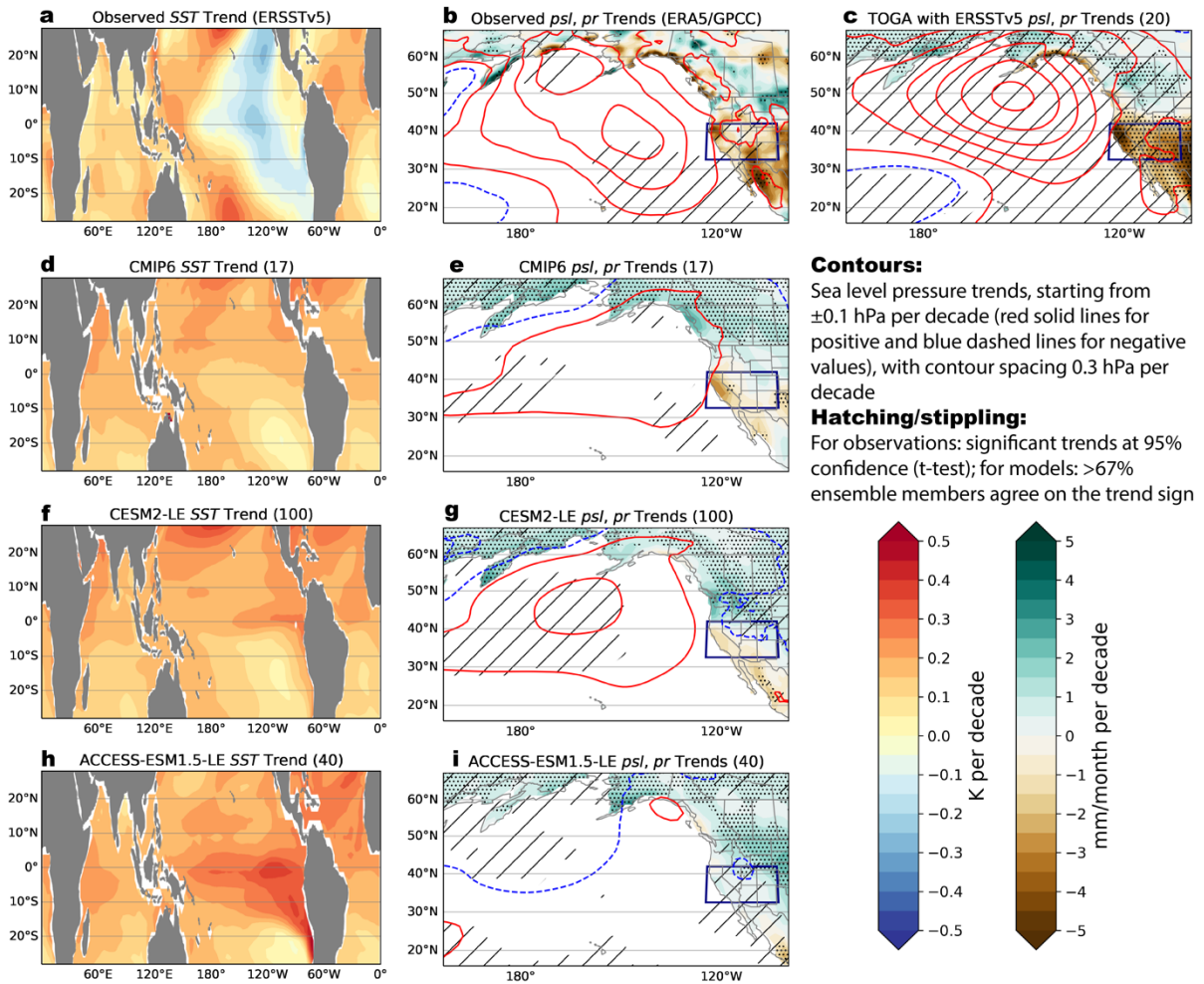
34 The Southwestern United States (SWUS) is a semi-arid region with Mediterranean
35 climate, in which precipitation mainly arrives during winter-spring (Dec-May, DJFMAM)
36 and is balanced by evaporative loss during hot and dry summers (Jun-Aug, JJA). In recent
37 decades, increasing freshwater demand from population growth, and agricultural and
38 industrial uses¹⁻⁴ has increased the vulnerability of the SWUS to droughts. Since about
39 the 1980s, the SWUS also shifted into drier conditions climatically^{5,6}. The combination of
40 declining winter-spring precipitation and rising summer air temperature⁶⁻¹⁰ led to reduced
41 soil moisture¹¹, increased vapor pressure deficit¹², enhanced wildfire risk^{13,14}, and
42 depleted reservoirs¹⁵. While past warming has been robustly attributed to anthropogenic
43 forcing⁶⁻⁹, it is uncertain to what extent the observed precipitation decline is externally
44 forced¹⁶⁻²⁰.

45 Much of the uncertainty in forced precipitation change is due to the uncertain estimate of
46 forced circulation change²¹⁻²³. The SWUS winter-spring precipitation correlates with the
47 strength of the Aleutian Low, a quasi-stationary low-pressure system over the North
48 Pacific²⁴. The Aleutian Low's variability can be influenced by anomalous heating from
49 tropical Pacific sea surface temperatures (SSTs) via planetary waves; on interannual time
50 scales this forms the well-studied teleconnection from the El Niño-Southern Oscillation
51 (ENSO) to SWUS precipitation^{6,19,25-27}. A similar mechanism applies to decadal time
52 scales^{28,29}. Therefore, the observed post-1980 weakening of the Aleutian Low and the
53 decreasing SWUS precipitation are frequently attributed to the observed La Niña-like
54 trend in tropical Pacific SSTs (Fig. 1a-1b)^{17,19,20,30,31}. This is confirmed by tropical ocean

55 global atmosphere (TOGA) simulations with atmosphere-land models forced with
56 observed tropical SSTs, which largely reproduce the pattern and strength of the observed
57 Aleutian Low and precipitation trends (Fig. 1c; extratropical SSTs have a negligible
58 influence, see Fig. S1). Given this pronounced influence of tropical SSTs on circulation
59 and precipitation, it is surprising to find that CMIP6 models, which simulate forced El Niño-
60 like SST trends in recent decades (at odds with observations; Fig. 1d; see also³²⁻³⁵), also
61 produce a weakening of the Aleutian Low and a decline in SWUS precipitation (Fig. 1e),
62 contrary to what would be expected based on El Niño-like SST trends alone. This
63 suggests that the recent North Pacific atmospheric circulation trend, and by extension the
64 SWUS precipitation decline, is partly forced but in a way that is not critically dependent
65 on the specific tropical SST pattern.

66 However, tropical SST trends can still modulate the influence of external forcing, such
67 that we might expect an El Niño-like tropical warming pattern to counteract the forced
68 North Pacific circulation change. For example, while a model with a modest El Niño-like
69 SST warming pattern similar to the CMIP6 ensemble mean (CESM2; Fig. 1f-g) also
70 shows a weakening of the Aleutian Low, a model with an exceptionally strong El Niño-
71 like SST trend (ACCESS-ESM1.5; Fig. 1f) does not, consistent with the expected
72 teleconnections associated with El Niño-like warming^{28,36,37}; though even in this case a
73 weak increase in sea level pressure remains over the Gulf of Alaska. Understanding how
74 historical forcings and tropical warming patterns, as independent drivers, influence trends
75 in the North Pacific sector is necessary to refine projections of near-future drought risk²⁹.
76 Here, we use a hierarchy of model simulations to investigate the roles of tropical SST
77 trends and direct radiative forcing on North Pacific circulation and SWUS hydroclimate

78 changes. We probe the possibility that the current SWUS drought has been more
 79 inevitable than previously thought, as both the temperature increase and the precipitation
 80 decline might have been partly forced.



81
 82 **Figure 1. Observed and simulated 1980-2014 DJFMAM trends in sea surface**
 83 **temperature (SST), sea level pressure (psl), and precipitation (pr).** Observed **a**, SST
 84 trend (ERSSTv5), **b**, psl and pr trends (ERA5/GPCC), **c**, 20-member ensemble mean
 85 from Tropical Ocean Global Atmosphere (TOGA) simulations (10-member CAM6/CLM5
 86 (CESM2), 10-member UM7.3/CABLE (ACCESS-ESM1.5)) prescribed with tropical SSTs
 87 from ERSSTv5. 17-model mean CMIP6 **d**, SST, and **e**, psl and pr trends. **f-g** and **h-i** are

88 similar to **d-e** but from 100-member CESM2-LE and 40-member ACCESS-ESM1.5-LE,
89 respectively. Hatching/Stippling marks *psl/pr* trends with 95% significant level for
90 observations, and when 67% of the ensemble members agree with the sign of the
91 ensemble mean for model simulations.

92

93 **Changing teleconnections from tropical decadal SST variability**

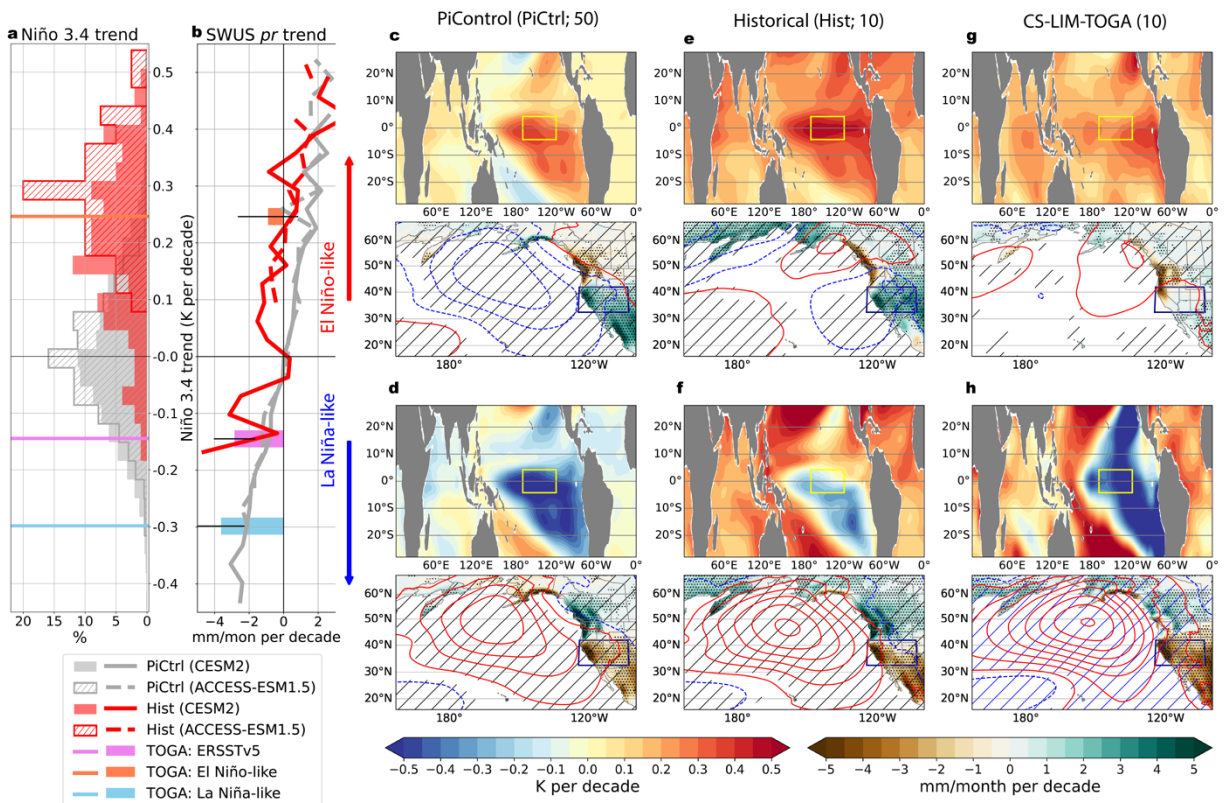
94 CESM2 and ACCESS-ESM1.5, as well as CMIP6 models more generally, tend to
95 produce an El Niño-like SST trend under historical forcing (Fig. 2a). However, these
96 models show a systematic shift towards lower SWUS precipitation trends during 1980-
97 2014 (*Historical*; hereafter *Hist*) compared with pre-industrial (*PiControl*; hereafter *PiCtrl*)
98 when binned by Niño 3.4 trends (Fig. 2a-2b; Methods). Specifically, the crossover point
99 between positive and negative SWUS precipitation trends occurs at Niño 3.4 trends of
100 ~ 0.2 K/decade for *Hist* rather than the expected 0 K/decade found in *PiCtrl*. In the
101 absence of external forcing (*PiCtrl*), the top decadal Niño 3.4 trends (above 97.5th/ below
102 2.5th percentiles for *PiCtrl*; see Methods) in tropical Pacific SSTs of both signs lead to the
103 canonical and symmetric modulation of atmospheric circulation and SWUS precipitation
104 trends: El Niño-like trends decrease sea level pressure over the North Pacific and
105 increase SWUS precipitation and vice versa for La Niña-like trends (Fig. 2c-2d for CESM2
106 and Fig. S2 for ACCESS-ESM1.5). Under 1980-2014 forcing (*Hist*), however, the sea
107 level pressure over the North Pacific tends to increase despite the El Niño-like SST trends
108 (Fig. 2e-2f for CESM2 and Fig. S2 for ACCESS-ESM1.5). Even in the strongest El Niño-
109 like members (Niño 3.4 trends above 90th percentiles; Methods), there is an increased
110 sea level pressure around the Gulf of Alaska, creating a circulation pattern distinct from

111 a canonical El Niño-like response and more conducive to precipitation declines further
112 south along the North American West Coast during canonical El Niño (Fig. 2e).
113 However, interpreting this systematic shift in tropical SST teleconnections in coupled
114 models is challenging. Results from coupled model simulations involve direct radiatively
115 forced changes (i.e., without SST changes), indirect radiatively forced changes (i.e., with
116 SST changes, such as uniform warming and patterned warming), and the interplay with
117 internal SST and atmospheric variability^{30,38}. Additionally, coupled models struggle to
118 capture the observed La Niña-like trend despite the sizable magnitude of internal
119 variability around their mean trend (Fig. 2a). To more robustly disentangle the influence
120 of SST trends and external forcing in the face of large internal atmospheric variability, we
121 create a set of counterfactual 20-member TOGA ensembles with CESM2 and ACCESS-
122 ESM1.5 (Fig. 2g-2h; Methods). The SST trajectories for each ensemble are generated
123 with a stochastically forced cyclostationary linear inverse model³⁹ (LIM; Methods), which
124 can create synthetic SSTs that preserve the spatial and temporal statistical properties of
125 observed variability^{25,29}. We create realizations with an El Niño-like and a La Niña-like
126 SST trend pattern (corresponding to Niño 3.4 trends of about +/-0.3 K/decade; Fig. 2a)
127 and prescribe the tropical portion of these SSTs to the atmosphere-land models, under
128 time-evolving radiative forcing, with climatological values for extratropical SSTs and sea
129 ice concentrations (termed LIM-TOGA simulations).

130 Surprisingly, even in the LIM-TOGA El Niño-like case, the North Pacific sea level pressure
131 increases slightly, inducing a precipitation decline over the U.S. Pacific Northwest
132 extending to the northwestern portion of the SWUS (Fig. 2g). Internal atmospheric
133 variability can still create positive SWUS precipitation trends, but drying trends are

134 substantially more likely in the LIM-TOGA El Niño-like case (65% vs 35% of members,
 135 pooling simulations from CESM2 and ACCESS-ESM1.5; not shown). In the LIM-TOGA
 136 La Niña-like case, we find the expected North Pacific sea level pressure increase and
 137 significant SWUS precipitation decline (Fig. 2h). Just like in the fully-coupled models,
 138 precipitation trends for the El Niño and La Niña LIM-TOGA realizations are systematically
 139 lower than those based on *PiCtrl* segments for the same Niño 3.4 trend values (Fig. 2b).
 140 These results confirm a North Pacific circulation change and associated SWUS drying
 141 beyond what would be expected from internally generated Niño 3.4 trends alone (i.e., the
 142 impact that Niño 3.4 trends have in *PiCtrl*).

143



144

145 **Figure 2. Impacts of tropical Pacific SST trends on DJFMAM North Pacific**
 146 **hydroclimate trends in different climate mean states. a, histograms of 34-year Niño**

147 3.4 trends from Observation (ERSSTv5; for TOGA: ERSSTv5), CS-LIM generated
148 synthetic SSTs (TOGA: El Niño-like and TOGA: La Niña-like), PiCtrl and Hist from CESM2
149 and ACCESS-ESM1.5. **b**, averaged 34-year SWUS pr trends binned by Niño 3.4 trends.
150 Black error bars around the bars from TOGA simulations are ± 1 standard deviation of the
151 variability across 20 ensemble members. (**c**, **e**, **g**), El Niño-like SST trends and associated
152 psl and pr responses in CESM2 from **c**, PiCtrl (50), **e**, Hist (10), and **g**, CS-LIM-TOGA
153 (10). (**d**, **f**, **h**) same as (**c**, **e**, **g**) but for La Niña-like SST trends. Hatching/Stippling
154 indicates psl/pr trends where 67% of the ensemble members agree with the sign of the
155 ensemble mean.

156

157 **Forced changes oppose the expected response from El Niño-like trend**

158 The systematic hydroclimate shift across different tropical SST trends and model
159 configurations implies an externally forced change in circulation. The negative correlation
160 between tropical Niño 3.4 SST trends and equatorial 200hPa velocity potential gradient
161 (VPG) trends (Methods), a metric that measures the initial step of the tropics-to-
162 extratropics teleconnection through the generation of tropical divergent flow, does not
163 change markedly from PiCtrl to the post-1980 period (Fig. 3a-3b). However, the
164 relationship between equatorial 200hPa VPG trends and the North Pacific Index (NPI;
165 Methods) trends changes in the post-1980 period (Fig. 3c), resulting in a shift toward
166 more positive trends in North Pacific sea level pressure regardless of tropical SST trends
167 (Fig. 3a).

168 Indeed, the El Niño-like tropical warming patterns under post-1980 historical forcings do
169 not look similar to the pre-industrial El Niño-like trends (Fig. 2c, 2e, 2g), due to the

170 widespread warming outside of the equatorial Pacific in the former but not the latter. To
171 decompose the individual drivers of the systematic hydroclimate shift, we examine the
172 impacts from transient post-1980 historical forcings alone (i.e., radiative forcing, with
173 climatological SSTs and sea ice, termed *RF only*), and time-slice experiments in which
174 the LIM-based El Niño-like SST trend pattern (termed *El Niño-like only*) and a uniform 2K
175 warming (termed *2K only*) are imposed within constant radiative forcing representative of
176 the year 2000 (Methods).

177 *RF only* triggers a weak anti-cyclonic response over the northern part of the Aleutian Low
178 but overall has little impact on SWUS precipitation (Fig. 3d). Such a radiatively forced
179 Aleutian Low response has previously been attributed to changes in aerosol
180 emissions^{30,40-43}. The CESM2 single forcing large ensemble confirms that this radiatively
181 forced anti-cyclonic response over the North Pacific is attributable to historical
182 anthropogenic aerosols (AAER; Fig. 3e-3f). However, it is worth noting that neither ocean
183 coupling nor Arctic sea ice changes are critically needed to form this radiatively forced
184 North Pacific anti-cyclonic response.

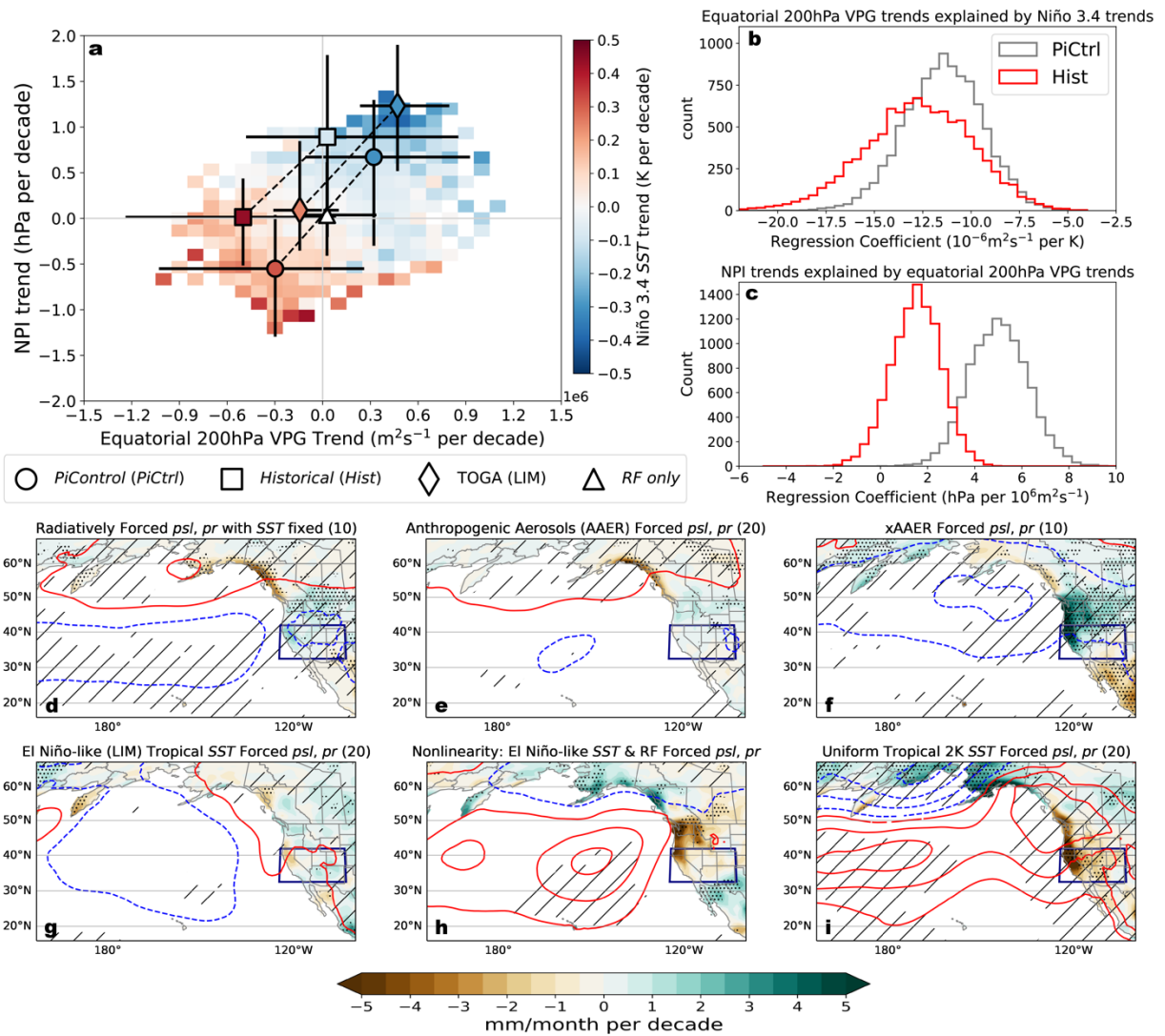
185 The *El Niño-like only* simulation, with radiative forcing held fixed at year 2000 levels, on
186 the other hand, does recover much of the circulation change over the Gulf of Alaska and
187 a coastal SWUS precipitation decline (Fig. 3g) as seen in the transient historical LIM-
188 TOGA simulations with the El Niño-like SST trend (Fig. 2g). However, it also retains a hint
189 of the canonical El Niño-like response with a slight deepening of the Aleutian Low.
190 Ultimately, the sum of *RF only* and *El Niño-like only* (Fig. 3h) does not completely recover
191 the behavior of the transient LIM-TOGA simulations with the El Niño-like SST trend,
192 suggesting a nonlinear interaction of these two drivers. The residual exhibits a broad

193 North Pacific sea level pressure increase and SWUS precipitation decline (Fig. 3h,
194 calculated as the difference between Fig. 2g and the sum of Fig. 3d and 3g). Such a
195 nonlinearity is reminiscent of the pattern difference between the trends in the fully coupled
196 CESM2 all-forcing historical simulations and the sum of AAER and xAAER simulations
197 (Fig. S3a), in which AAER creates relatively negligible tropical SST changes (Fig. S3b,
198 analogous to *RF only*) and xAAER creates an El Niño-like SST trend (Fig. S3c, analogous
199 to *El Niño-like only*). The unintuitive SWUS precipitation response under El Niño-like SST
200 trends thus arises from non-additive North Pacific circulation changes due to tropical
201 SSTs and direct radiative forcing, a behavior that is consistent across fully coupled and
202 SST-prescribed simulations based on CESM2.

203 Outside of the Eastern tropical Pacific, tropical SSTs exhibit robust overall warming as a
204 response to radiative forcing (Fig. 1d, 1f, 1h) and, unlike the Eastern tropical Pacific, are
205 not subject to large internal variability that can change the sign of the 1980-2014 trend
206 (Fig. 2e-2h). Indian and Atlantic Ocean warming has been identified as contributing to
207 SWUS drying^{29,31,44}. Therefore, we examine the contribution from uniform tropical
208 warming with *2K only* (Methods). Without the El Niño-like warming in the Eastern tropical
209 Pacific, *2K only* leads to broad increases in sea level pressure across the North Pacific
210 and consequently is a contributing factor to the decline in winter-spring SWUS
211 precipitation (Fig. 3i). This has been argued to result from the overall increased lower
212 tropospheric stability⁴⁵ (Fig. S4) while the SWUS drying has been argued to result from
213 an expansion of the Hadley Cell^{23,46,47}.

214 Thus, we conclude that radiative forcing contributes to an atmospheric circulation
215 response over the North Pacific directly (via *RF only*) and indirectly (via uniform tropical

216 warming as well as the interaction of patterned tropical SST trends with RF) that favors
 217 SWUS winter-spring precipitation declines. Importantly, these post-1980 contributions
 218 from radiative forcing are sufficient to counteract even the influence of a hypothetical El
 219 Niño-like SST trend.
 220



221
 222 **Figure 3. Tropical-North Pacific teleconnection shift due to different drivers in**
 223 **CESM2 (CAM6).** a, scatter plot of the ensemble mean equatorial 200hPa velocity
 224 potential gradient (VPG) trends (x-axis), North Pacific Index (NPI) trends (y-axis), and

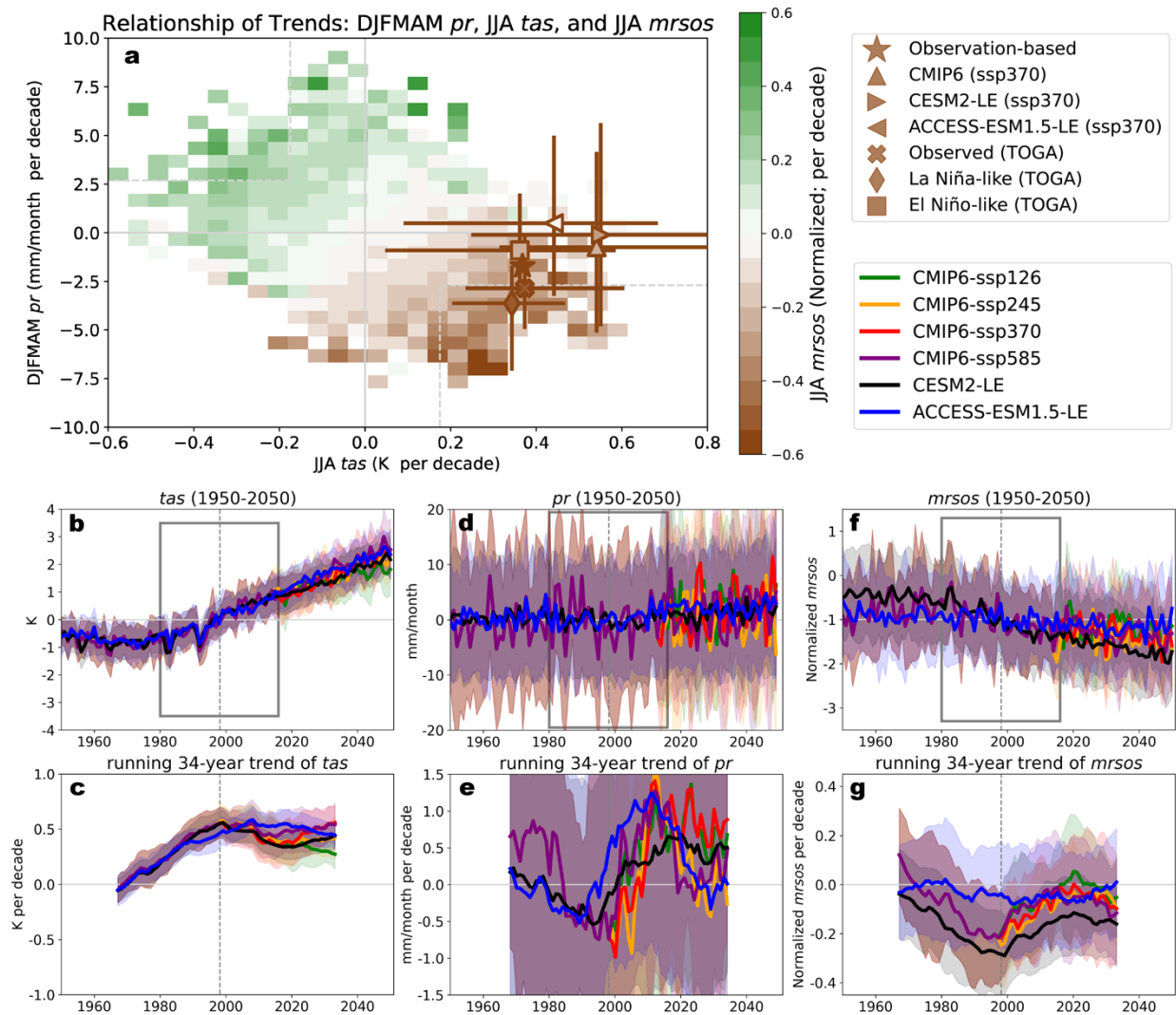
225 Niño 3.4 trends (color) from El Niño-like and La Niña-like members from different
226 simulations. The error bars are the full range of the ensemble members in each category.
227 The mesh grid shows the averaged Niño 3.4 trends binned by equatorial 200hPa VPG
228 trends and the NPI trends from PiCtrl. **b-c**, Regression coefficients from Hist and PiCtrl
229 simulations (vertical lines, solid/dashed lines for correlations with $p < 0.05$ / $p > 0.05$) and
230 their uncertainties from 10,000 bootstrapped regression coefficients (histograms) for **b**,
231 Niño 3.4 and equatorial 200hPa VPG trends and **c**, equatorial 200hPa VPG and NPI
232 trends. *psl* and *pr* trends driven by **d**, all post-1980 radiative forcing with fixed SSTs
233 representative of the average from 1880 to 2019 (RF only), **e**, anthropogenic aerosols
234 (AAER), **f**, everything-but-anthropogenic aerosols (xAAER), **g**, CS-LIM El Niño-like
235 warming (El Niño-like only) with fixed radiative forcings representative of 2000, **h**, the
236 nonlinearity from El Niño-like only and RF only (the difference between Fig. 2g and the
237 sum of Fig. 3d and Fig. 3g), and **i**, the uniform tropical 2K warming (2K only).
238 Hatching/Stippling is shown as *psl/pr* trends with 67% of the ensemble members agreeing
239 with the sign of the ensemble mean for model simulations.

240

241 **Implication for SWUS droughts**

242 Precipitation in DJFMAM is key in determining the drought risk for the SWUS in the
243 subsequent JJA dry season due to the snowmelt-driven nature of many of its
244 watersheds^{29,48,49}. We assess how the DJFMAM precipitation (*pr*) trend and the JJA air
245 temperature (*tas*) trend shape the risk of low JJA soil moisture (*mrsos*) over the SWUS.
246 Internally generated JJA soil moisture trends correlate with both DJFMAM precipitation
247 and JJA air temperature trends (PiCtrl, shown as mesh grid in Fig. 4a). PiCtrl also shows

248 a weak negative correlation between DJFMAM precipitation and JJA air temperature
249 trends, as the cold season precipitation can affect summertime air temperature through
250 land-atmosphere interactions and memory effects⁵⁰. The SWUS has experienced an
251 exceptional drying period since 1980 with a significant decline in JJA soil moisture (star
252 in Fig. 4a), also when compared with the strongest trends from *PiCtrl*. Decreasing
253 DJFMAM precipitation and increasing JJA air temperature contribute to the decline of the
254 JJA soil moisture, consistent with the relationship of these variables from *PiCtrl*. The
255 SWUS JJA air temperature increase is significant in observations and all TOGA
256 simulations (Fig. 4a). Together with the tendency for decreasing DJFMAM precipitation
257 independent of tropical Pacific SST trends, JJA soil moisture declines in almost all
258 historical simulations (except for *ACCESS-ESM1.5-LE*) for post-1980 (Fig. 4a). In other
259 words, the recent JJA SWUS soil moisture drought has been made substantially more
260 inevitable by the forced response of JJA temperature *and* cold season precipitation.
261 In fact, the DJFMAM precipitation decline, the JJA warming, and JJA soil moisture decline
262 over 1980-2014 are exceptional compared to other simulated 34-year periods in the past
263 and near future (Fig. 4b-4g). CESM2 and other CMIP6 models agree that the current
264 rates of change for all three quantities are at or near a local maximum, conspiring to make
265 this period one of exceptionally rapid change (Fig. 4c,e,g). While soil moisture is projected
266 to continue to decline under all emissions scenarios (Fig. 4g), its drying rate might be
267 alleviated somewhat by a reversal of the precipitation trend (Fig. 4e), either in response
268 to a projected strengthening of the El Niño-like warming⁵¹ due to greenhouse
269 gases^{28,29,36,37} and/or less aerosol emissions relative to the 1980s in all future scenarios⁵².
270



271
 272 **Figure 4. The relationship between SWUS DJFMAM pr trends, JJA tas trends, and**
 273 **JJA mrsos trends for 1980-2014 and future projections. a, the relationship between**
 274 **JJA tas trends (x-axis), DJFMAM pr trends (y-axis), and JJA mrsos trends (color) for**
 275 **1980-2014 from observation-based data, PiCtrl, Hist (CESM2-LE, ACCESS-ESM1.5-LE,**
 276 **CMIP6), and TOGA simulations. The error bars are the full range of the ensemble. The**
 277 **mesh grid shows the averaged JJA mrsos trends binned by JJA tas trends and DJFMAM**
 278 **pr trends from all PiCtrl segments. The time series of SWUS averaged b, tas, d, pr, f,**
 279 **mrsos (shown as anomalies from 1980-2014 climatological mean) of and the running 34-**

280 *year trends for SWUS averaged c, tas, e, pr, g, mrsos for 1950-2050. Shading in b-g is*
281 *the range of ± 1 standard deviation across ensemble members.*

282

283 **Discussion**

284 Projected North Pacific circulation and SWUS precipitation changes have previously been
285 linked to the Pacific SST warming pattern^{22,28,53}. Given its importance for various global
286 climate impacts, the observation-model discrepancy in the pattern of tropical Pacific SST
287 trends introduces substantial uncertainty to historical attribution and future projections.
288 Several hypotheses for the recent La Niña-like SST trend have been proposed, including
289 an internal shift of Pacific decadal variability⁵⁴, an amplification of the climatological
290 pattern by preferential warming of the Western over the Eastern Pacific⁵⁵, a delayed
291 response to GHG forcing due to the ocean thermostat effect⁵⁶, anthropogenic aerosol
292 forcing⁵⁷, Antarctic stratospheric ozone forcing⁵⁸, teleconnections from the Southern
293 Ocean⁵⁹⁻⁶¹ and equatorial upwelling⁶². Some of these hypotheses predict a future reversal
294 of the observed trend. In addition, the magnitude of the uniform SST warming can also
295 influence the tropical circulation and the North Pacific teleconnection pattern^{28,37,63,64}. Our
296 results here further complicate this story by providing evidence that the influence of the
297 tropical Pacific pattern of SST trends can be modulated in impactful but perhaps
298 unintuitive ways by direct radiatively forced atmospheric circulation change as well as
299 other aspects of the global warming signal, such as uniform warming. Not addressed here
300 but potentially also of importance are uncertainties in projected changes of the North
301 American summer monsoon⁶⁵ and its influence on water resources in the SWUS.
302 Ultimately, a better understanding of the tug-of-war between the radiatively forced North

303 Pacific circulation change, either directly from radiative forcing or indirectly through
304 tropical SST warming patterns and mean warming, and the interplay with internally-
305 generated SST trends, as well as their cause and thus likely future trajectory, is key to
306 robustly projecting future SWUS hydroclimate change.

307

308 **Methods**

309 ***Data***

310 For observational data, we take monthly sea surface temperature (SST) from ERSSTv5⁶⁶,
311 precipitation from Global Precipitation Climatology Centre⁶⁷, sea-level pressure from
312 ERA5⁶⁸, surface soil moisture from GLEAMv3.7⁶⁹, and near-surface air temperature over
313 land from Berkeley Earth⁷⁰. We regrid observational datasets to the CESM2 native
314 nominal 1° latitude/longitude grid. We use sea surface temperature (*tos*), near-surface air
315 temperature (*tas*), precipitation (*pr*), sea level pressure (*psl*), and soil moisture (*mrsos*)
316 from the 100-member Community Earth System Model version 2 large ensemble
317 (CESM2-LE⁷¹), the 20-member anthropogenic-aerosols-only (AAER) and the 10-member
318 everything-but-anthropogenic aerosols (xAAER) single forcing simulations⁷², and the
319 2000-year long pre-industrial simulation (*PiCtrl*) of CESM2⁷³. *mrsos* values are
320 normalized as z-score (mean removed and divided by the standard deviation of
321 interannual variability)⁷⁴. We also include the 40-member ACCESS-ESM1.5 large
322 ensemble (ACCESS-ESM1.5 LE⁷⁵) and its 900-year *PiCtrl* simulation. We follow previous
323 studies to remove the long-term drift in *PiCtrl* through linear detrending³⁰. Seventeen
324 other models from the Coupled Model Intercomparison Project Phase 6 (CMIP6⁷⁶) with
325 all four future SSP scenarios are also included (See Supplementary Table 1), as well as

326 the last 300-year of their *PiCtrl* simulations. The CMIP6 and ACCESS-ESM1.5 LE outputs
327 are regridded to a 2.5° grid.

328

329 ***Atmospheric General Circulation Model (AGCM) experiments***

330 Two kinds of tropical ocean global atmosphere (TOGA) AGCM experiments were
331 conducted for this study, including transient historical simulations (i.e., time-evolving
332 radiative forcing) and simulations with a particular SST pattern and radiative forcing held
333 fixed. TOGA simulations prescribe time-evolving SSTs within 28°N/S and 1880-2019
334 climatological seasonal cycle of SSTs from 35°S/N polewards, with a linear interpolation
335 of SSTs between 28°N/S and 35°N/S. The sea ice forcing is held as an 1880-2019
336 climatological seasonal cycle for all TOGA experiments.

337 For the transient historical TOGA experiments, we use existing experiments from CESM2
338 (CAM6 for the atmosphere and CLM5 for the land) and ACCESS-ESM1.5 (UM for the
339 atmosphere and CABLE for the land) to generate a 20-member ensemble (10-member
340 for each model) of AGCM simulations with prescribed observed tropical SSTs from
341 ERSSTv5. In addition, two new 20-member TOGA experiments are conducted with time-
342 evolving synthetic SSTs, one with an *El Niño-like* (Fig. 2g) and the other with a *La Niña-*
343 *like* (Fig. 2h) trend pattern, generated from a cyclostationary linear inverse model (CS-
344 LIM³⁹) trained on observations (termed LIM-TOGA simulations). These LIM-generated
345 SST trajectories include a representation of internal variability and an estimate of the
346 forced response found in observations. Details about the creation of the synthetic SSTs
347 with CS-LIM can be found in the Supplementary Information. All three experiments
348 prescribe the same climatological sea ice from HadISST1 and CMIP6 historical forcings

349 (note that in CAM6, we prescribe the smoothed biomass burning version of CMIP6
350 historical forcings, CMIP6smbb^{77,78}).

351 Sensitivity experiments with CAM6 are used to identify the impacts from direct radiative
352 forcing (*RF*), tropical *El Niño-like* patterned warming (*El Niño-like only*), and 2K uniform
353 tropical warming (*2K only*). *RF* is conducted as a 10-member ensemble with the same
354 CMIP6smbb historical forcings as the TOGA simulations but with 1880-2019
355 climatological SSTs and sea ice everywhere. The *El Niño-like only* and *2K only*
356 experiments are constructed differently: we conduct three 23-year CAM6 simulations with
357 radiative forcings fixed as 2000 level (F2000climo) with the last 21 years used for
358 analyses (20 samples of DJFMAM). These F2000climo runs include one control run
359 forced with the 1880-2019 climatological SSTs and sea ice everywhere. The other two
360 runs are forced by the same climatological SSTs and sea ice but (i) adding the *El Niño-*
361 *like* annual mean SST linear trend (termed *El Niño-like only*, trend calculated from the
362 1980-2014 annual mean SST of the *El Niño-like* LIM-TOGA experiment, including internal
363 variability and the estimated forced response, in unit of K per 35 years) and (ii) adding the
364 2K uniform warming (*2K only*). The difference between the perturbation runs and the
365 control run isolates the impact of *El Niño-like* warming and 2K warming, respectively^{79,80}.

366

367 ***Definitions for indices and regional mean quantities***

368 Niño 3.4 is calculated as the average SST over the domain of 5°S–5°N, 170°W–120°W
369 (yellow box shown in the SST trend maps). We define SWUS using the domain 32.5–
370 42°N, 102.5–125°W (land-only; navy box shown in *psl*, *pr* trend maps). The equatorial
371 200hPa velocity potential gradient (VPG) is defined as the difference between the

372 equatorial eastern Pacific (5°S–5°N, 180°W–137.5°W) and the equatorial western Pacific
373 (5°S–5°N, 110°E–180°E). The North Pacific Index (NPI) is defined as the sea level
374 pressure averaged over 30–65°N, 160°E–140°W. All indices are calculated as area-
375 weighted means.

376

377 ***The selection of strong decadal trends according to Niño 3.4 SST trends***

378 We bin the Niño 3.4 SST trends from *Historical (Hist)* and *PiCtrl* for CESM2 and ACCESS-
379 ESM1.5 into 30 bins, respectively. The 30 bins are evenly spaced between the maxima
380 and minima of all possible Niño 3.4 SST trends pooled from *Hist* and *PiCtrl* simulations
381 from both CESM2 and ACCESS-ESM1.5. Then, we sort the SWUS winter-spring
382 (DJFMAM) precipitation trends into the 30 bins according to their Niño 3.4 SST trends
383 and show the averaged SWUS winter-spring precipitation trend for that Niño 3.4 SST
384 trend bin (red and gray lines in Fig. 2b). We create composite maps of top La Niña-like/El
385 Niño-like SSTs and their teleconnections (Fig. 2) based on the ensemble members with
386 Niño 3.4 trends below the 2.5th/ above the 97.5th percentiles in *PiCtrl* and below the 10th/
387 above the 90th percentiles in *Hist*.

388

389 ***Bootstrapping to estimate the uncertainty of regression coefficients***

390 We randomly select 100 members from the *PiCtrl* and *Hist* simulations from CESM2 for
391 Niño 3.4 trends, equatorial 200hPa VPG trends, and NPI trends and repeat this procedure
392 10,000 times to account for the uncertainty of the regression coefficients between these
393 quantities.

394

395 ***Nonlinear effects in trends***

396 The nonlinear effect in *psl*, *pr* trends from interactions between anthropogenic aerosols
397 (AAER) and forcings other than anthropogenic aerosols (xAAER) in fully coupled
398 simulations is calculated as

399
$$X_{nl} = X_{ALL} - X_{AAER} - X_{xAAER}$$

400 X_{ALL} refers to the trends from the all forcings *Hist* simulation, X_{AAER} the trends from AAER
401 simulation, and X_{xAAER} the trends from the xAAER simulation.

402 The nonlinear effect in *psl*, *pr* trends from interactions between radiatively forced
403 response (mainly by anthropogenic aerosols) and the El Niño-like SST trend (mainly by
404 greenhouse gases, included in xAAER) in AGCM simulations is calculated as

405
$$X_{nl} = X_{TOGA:El\ Ni\tilde{n}o-like} - X_{El\ Ni\tilde{n}o-like\ only} - X_{RF}$$

406 Where $X_{TOGA:El\ Ni\tilde{n}o-like}$ refers to the trends from the LIM-TOGA simulations with time
407 evolving El Niño-like trends and time evolving radiative forcing, $X_{El\ Ni\tilde{n}o-like\ only}$ the
408 anomalous change caused by the El Niño-like trend, and X_{RF} the trend from radiative
409 forcing when SSTs are held fixed. Since the number of ensemble members differs
410 between the ensembles, we bootstrap members in each ensemble 100 times to create a
411 100-member X_{nl} for calculating signal-to-noise ratio (S/N).

412 **Reference**

- 413 1. Gleick, P. H. Roadmap for sustainable water resources in southwestern North America.
414 *Proc. Natl. Acad. Sci. U.S.A.* **107**, 21300–21305 (2010).
- 415 2. Gleick, P. *Impacts of California's Ongoing Drought: Hydroelectricity Generation*.
416 (2016).
- 417 3. Medellín-Azuara, J., MacEwan, D., Howitt, R. E. & Sumner, D. A. *A Report for the*
418 *California Department of Food and Agriculture*. (2016).
- 419 4. Lund, J., Medellín-Azuara, J., Durand, J. & Stone, K. Lessons from California's 2012–
420 2016 Drought. *J. Water Resour. Plann. Manage.* **144**, 04018067 (2018).
- 421 5. Prein, A. F., Holland, G. J., Rasmussen, R. M., Clark, M. P. & Tye, M. R. Running dry:
422 The U.S. Southwest's drift into a drier climate state. *Geophysical Research Letters* **43**,
423 1272–1279 (2016).
- 424 6. Lehner, F., Deser, C., Simpson, I. R. & Terray, L. Attributing the U.S. Southwest's
425 Recent Shift Into Drier Conditions. *Geophys. Res. Lett.* **45**, 6251–6261 (2018).
- 426 7. Diffenbaugh, N. S., Swain, D. L. & Touma, D. Anthropogenic warming has increased
427 drought risk in California. *Proc. Natl. Acad. Sci. U.S.A.* **112**, 3931–3936 (2015).
- 428 8. Williams, A. P. *et al.* Large contribution from anthropogenic warming to an emerging
429 North American megadrought. *Science* **368**, 314–318 (2020).
- 430 9. Williams, A. P., Cook, B. I. & Smerdon, J. E. Rapid intensification of the emerging
431 southwestern North American megadrought in 2020–2021. *Nat. Clim. Chang.* **12**, 232–
432 234 (2022).
- 433 10. Seager, R. *et al.* Mechanisms of a meteorological drought onset: summer 2020 to
434 spring 2021 in southwestern North America. *Journal of Climate* 1–36 (2022)
435 doi:10.1175/JCLI-D-22-0314.1.
- 436 11. Ault, T. R., Mankin, J. S., Cook, B. I. & Smerdon, J. E. Relative impacts of mitigation,
437 temperature, and precipitation on 21st-century megadrought risk in the American
438 Southwest. *Sci. Adv.* **2**, e1600873 (2016).
- 439 12. Juang, C. S. *et al.* Rapid Growth of Large Forest Fires Drives the Exponential
440 Response of Annual Forest-Fire Area to Aridity in the Western United States. *Geophysical*
441 *Research Letters* **49**, e2021GL097131 (2022).

- 442 13. Jacobson, T. W. P., Seager, R., Williams, A. P. & Henderson, N. Climate Dynamics
443 Preceding Summer Forest Fires in California and the Extreme Case of 2018. *Journal of*
444 *Applied Meteorology and Climatology* **61**, 989–1002 (2022).
- 445 14. Jacobson, T. W. P. *et al.* An Unexpected Decline in Spring Atmospheric Humidity in
446 the Interior Southwestern United States and Implications for Forest Fires. *Journal of*
447 *Hydrometeorology* **25**, 373–390 (2024).
- 448 15. Lukas, J. & Payton, E. *Colorado River Basin Climate and Hydrology: State of the*
449 *Science*. (2020).
- 450 16. Pierce, D. W. *et al.* The Key Role of Heavy Precipitation Events in Climate Model
451 Disagreements of Future Annual Precipitation Changes in California. *Journal of Climate*
452 **26**, 5879–5896 (2013).
- 453 17. Delworth, T. L., Zeng, F., Rosati, A., Vecchi, G. A. & Wittenberg, A. T. A Link between
454 the Hiatus in Global Warming and North American Drought. *Journal of Climate* **28**, 3834–
455 3845 (2015).
- 456 18. Polade, S. D., Gershunov, A., Cayan, D. R., Dettinger, M. D. & Pierce, D. W.
457 Precipitation in a warming world: Assessing projected hydro-climate changes in California
458 and other Mediterranean climate regions. *Sci Rep* **7**, 10783 (2017).
- 459 19. Seager, R. & Ting, M. Decadal Drought Variability Over North America: Mechanisms
460 and Predictability. *Curr Clim Change Rep* **3**, 141–149 (2017).
- 461 20. Seager, R. *et al.* Climate Variability and Change of Mediterranean-Type Climates.
462 *Journal of Climate* **32**, 2887–2915 (2019).
- 463 21. Shepherd, T. G. Atmospheric circulation as a source of uncertainty in climate change
464 projections. *Nature Geosci* **7**, 703–708 (2014).
- 465 22. Choi, J., Lu, J., Son, S., Frierson, D. M. W. & Yoon, J. Uncertainty in future projections
466 of the North Pacific subtropical high and its implication for California winter precipitation
467 change. *J. Geophys. Res. Atmos.* **121**, 795–806 (2016).
- 468 23. Schmidt, D. F. & Grise, K. M. The Response of Local Precipitation and Sea Level
469 Pressure to Hadley Cell Expansion. *Geophysical Research Letters* **44**, (2017).
- 470 24. Horel, J. & Wallace, J. Planetary-Scale Atmospheric Phenomena Associated with the
471 Southern Oscillation. 813–829 (1981) doi:[https://doi.org/10.1175/1520-](https://doi.org/10.1175/1520-0493(1981)109<0813:PSAPAW>2.0.CO;2)
472 [0493\(1981\)109<0813:PSAPAW>2.0.CO;2](https://doi.org/10.1175/1520-0493(1981)109<0813:PSAPAW>2.0.CO;2).

- 473 25. Carrillo, C. M. *et al.* Megadrought: A Series of Unfortunate La Niña Events? *JGR*
474 *Atmospheres* **127**, e2021JD036376 (2022).
- 475 26. Seager, R., Kushnir, Y., Herweijer, C., Naik, N. & Velez, J. Modeling of Tropical
476 Forcing of Persistent Droughts and Pluvials over Western North America: 1856–2000*.
477 *Journal of Climate* **18**, 4065–4088 (2005).
- 478 27. Seager, R. & Hoerling, M. Atmosphere and Ocean Origins of North American
479 Droughts*. *Journal of Climate* **27**, 4581–4606 (2014).
- 480 28. Allen, R. J. & Luptowitz, R. El Niño-like teleconnection increases California
481 precipitation in response to warming. *Nat Commun* **8**, 16055 (2017).
- 482 29. Seager, R. *et al.* Ocean-forcing of cool season precipitation drives ongoing and future
483 decadal drought in southwestern North America. *npj Clim Atmos Sci* **6**, 141 (2023).
- 484 30. Kuo, Y., Kim, H. & Lehner, F. Anthropogenic Aerosols Contribute to the Recent
485 Decline in Precipitation Over the U.S. Southwest. *Geophysical Research Letters* **50**,
486 e2023GL105389 (2023).
- 487 31. Hoerling, M. & Kumar, A. The Perfect Ocean for Drought. *Science* **299**, 691–694
488 (2003).
- 489 32. Wills, R. C. J., Dong, Y., Proistosescu, C., Armour, K. C. & Battisti, D. S. Systematic
490 Climate Model Biases in the Large-Scale Patterns of Recent Sea-Surface Temperature
491 and Sea-Level Pressure Change. *Geophysical Research Letters* **49**, (2022).
- 492 33. Seager, R., Henderson, N. & Cane, M. Persistent Discrepancies between Observed
493 and Modeled Trends in the Tropical Pacific Ocean. *Journal of Climate* **35**, 4571–4584
494 (2022).
- 495 34. Rugenstein, M. *et al.* Connecting the SST Pattern Problem and the Hot Model
496 Problem. *Geophysical Research Letters* **50**, e2023GL105488 (2023).
- 497 35. Coats, S. & Karnauskas, K. B. Are Simulated and Observed Twentieth Century
498 Tropical Pacific Sea Surface Temperature Trends Significant Relative to Internal
499 Variability? *Geophysical Research Letters* **44**, 9928–9937 (2017).
- 500 36. Gan, B. *et al.* On the Response of the Aleutian Low to Greenhouse Warming. *Journal*
501 *of Climate* **30**, 3907–3925 (2017).
- 502 37. Dong, L. & Leung, L. R. Winter Precipitation Changes in California Under Global
503 Warming: Contributions of CO₂, Uniform SST Warming, and SST Change Patterns.
504 *Geophysical Research Letters* **48**, (2021).

- 505 38. Lehner, F. & Deser, C. Origin, importance, and predictive limits of internal climate
506 variability. *Environ. Res.: Climate* **2**, 023001 (2023).
- 507 39. Shin, S.-I., Sardeshmukh, P. D., Newman, M., Penland, C. & Alexander, M. A. Impact
508 of Annual Cycle on ENSO Variability and Predictability. *Journal of Climate* **34**, 171–193
509 (2021).
- 510 40. Smith, D. M. *et al.* Role of volcanic and anthropogenic aerosols in the recent global
511 surface warming slowdown. *Nature Clim Change* **6**, 936–940 (2016).
- 512 41. Dow, W. J., Maycock, A. C., Lofverstrom, M. & Smith, C. J. The Effect of
513 Anthropogenic Aerosols on the Aleutian Low. *Journal of Climate* **34**, 1725–1741 (2021).
- 514 42. Oudar, T., Kushner, P. J., Fyfe, J. C. & Sigmond, M. No Impact of Anthropogenic
515 Aerosols on Early 21st Century Global Temperature Trends in a Large Initial-Condition
516 Ensemble. *Geophys. Res. Lett.* **45**, 9245–9252 (2018).
- 517 43. Dittus, A. J., Hawkins, E., Robson, J. I., Smith, D. M. & Wilcox, L. J. Drivers of Recent
518 North Pacific Decadal Variability: The Role of Aerosol Forcing. *Earth's Future* **9**, (2021).
- 519 44. Kushnir, Y., Seager, R., Ting, M., Naik, N. & Nakamura, J. Mechanisms of Tropical
520 Atlantic SST Influence on North American Precipitation Variability*. *Journal of Climate* **23**,
521 5610–5628 (2010).
- 522 45. Xu, M., Zhan, R. & Zhao, J. Distinct responses of tropical cyclone activity to spatio-
523 uniform and nonuniform SST warming patterns. *Environ. Res. Lett.* **19**, 064020 (2024).
- 524 46. Lu, J., Vecchi, G. A. & Reichler, T. Expansion of the Hadley cell under global warming.
525 *Geophysical Research Letters* **34**, 2006GL028443 (2007).
- 526 47. Zhou, C., Lu, J., Hu, Y. & Zelinka, M. D. Responses of the Hadley Circulation to
527 Regional Sea Surface Temperature Changes. *Journal of Climate* **33**, 429–441 (2020).
- 528 48. St. George, S., Meko, D. M. & Cook, E. R. The seasonality of precipitation signals
529 embedded within the North American Drought Atlas. *The Holocene* **20**, 983–988 (2010).
- 530 49. Baek, S. H. *et al.* Precipitation, Temperature, and Teleconnection Signals across the
531 Combined North American, Monsoon Asia, and Old World Drought Atlases. *Journal of*
532 *Climate* **30**, 7141–7155 (2017).
- 533 50. Vargas Zeppetello, L. R., Zhang, L. N., Battisti, D. S. & Laguë, M. M. How Much Does
534 Land-Atmosphere Coupling Influence Summertime Temperature Variability in the
535 Western United States? *Journal of Climate* (2024) doi:10.1175/JCLI-D-23-0716.1.

- 536 51. Alessi, M. J. & Rugenstein, M. Potential Near-Term Wetting of the Southwestern
537 United States if the Eastern and Central Pacific Cooling Trend Reverses. *Geophysical*
538 *Research Letters* **51**, e2024GL108292 (2024).
- 539 52. Persad, G. G., Samset, B. H. & Wilcox, L. J. Aerosols must be part of climate risk
540 assessments.
- 541 53. Qiu, W., Collins, M., Scaife, A. A. & Santoso, A. Tropical Pacific trends explain the
542 discrepancy between observed and modelled rainfall change over the Americas. *npj Clim*
543 *Atmos Sci* **7**, (2024).
- 544 54. Chung, E.-S. *et al.* Reconciling opposing Walker circulation trends in observations
545 and model projections. *Nat. Clim. Chang.* **9**, 405–412 (2019).
- 546 55. Seager, R. *et al.* Strengthening tropical Pacific zonal sea surface temperature gradient
547 consistent with rising greenhouse gases. *Nat. Clim. Chang.* **9**, 517–522 (2019).
- 548 56. Heede, U. K. & Fedorov, A. V. Eastern equatorial Pacific warming delayed by aerosols
549 and thermostat response to CO₂ increase. *Nat. Clim. Chang.* **11**, 696–703 (2021).
- 550 57. Hwang, Y.-T., Xie, S.-P., Chen, P.-J., Tseng, H.-Y. & Deser, C. Contribution of
551 anthropogenic aerosols to persistent La Niña-like conditions in the early 21st century.
552 *Proc. Natl. Acad. Sci. U.S.A.* **121**, e2315124121 (2024).
- 553 58. Hartmann, D. L. The Antarctic ozone hole and the pattern effect on climate sensitivity.
554 *Proc. Natl. Acad. Sci. U.S.A.* **119**, e2207889119 (2022).
- 555 59. Kim, H., Kang, S. M., Kay, J. E. & Xie, S.-P. Subtropical clouds key to Southern Ocean
556 teleconnections to the tropical Pacific. *Proc. Natl. Acad. Sci. U.S.A.* **119**, e2200514119
557 (2022).
- 558 60. Dong, Y., Armour, K. C., Battisti, D. S. & Blanchard-Wrigglesworth, E. Two-Way
559 Teleconnections between the Southern Ocean and the Tropical Pacific via a Dynamic
560 Feedback. *Journal of Climate* **35**, 6267–6282 (2022).
- 561 61. Kang, S. M. *et al.* Global impacts of recent Southern Ocean cooling. *Proc. Natl. Acad.*
562 *Sci. U.S.A.* **120**, e2300881120 (2023).
- 563 62. Kohyama, T., Hartmann, D. L. & Battisti, D. S. La Niña-like Mean-State Response to
564 Global Warming and Potential Oceanic Roles. *Journal of Climate* **30**, 4207–4225 (2017).
- 565 63. Shin, S.-I. & Sardeshmukh, P. D. Critical influence of the pattern of Tropical Ocean
566 warming on remote climate trends. *Clim Dyn* **36**, 1577–1591 (2011).

- 567 64. Watanabe, M., Iwakiri, T., Dong, Y. & Kang, S. M. Two Competing Drivers of the
568 Recent Walker Circulation Trend. *Geophysical Research Letters* **50**, e2023GL105332
569 (2023).
- 570 65. Schmidt, D. F. & Grise, K. M. Impacts of Subtropical Highs on Summertime
571 Precipitation in North America. *J. Geophys. Res. Atmos.* **124**, 11188–11204 (2019).
- 572 66. Huang, B. *et al.* Extended Reconstructed Sea Surface Temperature, Version 5
573 (ERSSTv5): Upgrades, Validations, and Intercomparisons. *Journal of Climate* **30**, 8179–
574 8205 (2017).
- 575 67. Schneider, U., Hänsel, S., Finger, P., Rustemeier, E. & Ziese, M. GPCP Full Data
576 Monthly Product Version 2022 at 1.0°: Monthly Land-Surface Precipitation from Rain-
577 Gauges built on GTS-based and Historical Data.
578 https://doi.org/10.5676/DWD_GPCP/FD_M_V2022_100 (2022).
- 579 68. Hersbach, H. *et al.* The ERA5 global reanalysis. *Q.J.R. Meteorol. Soc.* **146**, 1999–
580 2049 (2020).
- 581 69. Martens, B. *et al.* GLEAM v3: satellite-based land evaporation and root-zone soil
582 moisture. *Geosci. Model Dev.* **10**, 1903–1925 (2017).
- 583 70. Rohde, R. A. & Hausfather, Z. The Berkeley Earth Land/Ocean Temperature Record.
584 *Earth Syst. Sci. Data* **12**, 3469–3479 (2020).
- 585 71. Rodgers, K. B. *et al.* Ubiquity of human-induced changes in climate variability. *Earth*
586 *Syst. Dynam.* **12**, 1393–1411 (2021).
- 587 72. Simpson, I. R. *et al.* The CESM2 Single-Forcing Large Ensemble and Comparison to
588 CESM1: Implications for Experimental Design. *Journal of Climate* **36**, 5687–5711 (2023).
- 589 73. Danabasoglu, G. *et al.* The Community Earth System Model Version 2 (CESM2). *J.*
590 *Adv. Model. Earth Syst.* **12**, (2020).
- 591 74. Cook, B. I. *et al.* Uncertainties, Limits, and Benefits of Climate Change Mitigation for
592 Soil Moisture Drought in Southwestern North America. *Earth's Future* **9**, e2021EF002014
593 (2021).
- 594 75. Ziehn, T. *et al.* The Australian Earth System Model: ACCESS-ESM1.5. *J. South.*
595 *Hemisph. Earth Syst. Sci.* **70**, 193–214 (2020).
- 596 76. Eyring, V. *et al.* Overview of the Coupled Model Intercomparison Project Phase 6
597 (CMIP6) experimental design and organization. *Geosci. Model Dev.* **9**, 1937–1958
598 (2016).

- 599 77. DeRepentigny, P. Enhanced simulated early 21st century Arctic sea ice loss due to
600 CMIP6 biomass burning emissions. *SCIENCE ADVANCES* (2022).
- 601 78. Fasullo, J. T. *et al.* Spurious Late Historical-Era Warming in CESM2 Driven by
602 Prescribed Biomass Burning Emissions. *Geophysical Research Letters* **49**,
603 e2021GL097420 (2022).
- 604 79. Yang, W., Hsieh, T.-L. & Vecchi, G. A. Hurricane annual cycle controlled by both
605 seeds and genesis probability. *Proc. Natl. Acad. Sci. U.S.A.* **118**, e2108397118 (2021).
- 606 80. Hsieh, T., Yang, W., Vecchi, G. A. & Zhao, M. Model Spread in the Tropical Cyclone
607 Frequency and Seed Propensity Index Across Global Warming and ENSO-Like
608 Perturbations. *Geophysical Research Letters* **49**, e2021GL097157 (2022).
- 609 81. Balmaseda, M. A., Mogensen, K. & Weaver, A. T. Evaluation of the ECMWF ocean
610 reanalysis system ORAS4. *Quart J Royal Meteoro Soc* **139**, 1132–1161 (2013).
- 611 82. Penland, C. & Matrosova, L. Studies of El Niño and Interdecadal Variability in Tropical
612 Sea Surface Temperatures Using a Nonnormal Filter. *Journal of Climate* **19**, 5796–5815
613 (2006).

614 **Acknowledgments**

615 We thank Wenchang Yang for helpful discussion. YK and FL were supported by NOAA
616 MAPP award NA21OAR4310349. FL acknowledges support from the U.S. Department
617 of Energy, Office of Science, Office of Biological & Environmental Research (BER),
618 Regional and Global Model Analysis (RGMA) component of the Earth and Environmental
619 System Modeling Program under Award Number DE-SC0022070 and National Science
620 Foundation (NSF) IA 1947282. IRS, CD, and ASP acknowledge funding from the NSF
621 National Center for Atmospheric Research (NCAR) which is a major facility sponsored by
622 the National Science Foundation under cooperative agreement No. 1852977. IRS also
623 acknowledges support from NOAA MAPP awards NA20OAR4310413 and
624 NA23OAR4310634. We also acknowledge the CESM Climate Variability and Change
625 Working group for making available the regular CESM TOGA, AAER and xAAER
626 simulations used in this work. Simulations were conducted on UCAR's supercomputers
627 Cheyenne (doi:10.5065/D6RX99HX) and Derecho (doi:10.5065/qx9a-pg09), operated by
628 NCAR's Computational and Information Systems Laboratory.

629 **Corresponding author**

630 Yan-Ning Kuo (yk545@cornell.edu)

631

632 **Author contributions**

633 Y.-N. K., F. L., C. D., M. N., I. R. S. conceptualized this study and the experimental set-
634 ups. M. N. and S.-I. S. generated the synthetic sea surface temperature (SST) with the
635 linear inverse model. Y.-N. K., A. S. P., S. W. conducted the prescribed SST experiments
636 (LIM-TOGA and F2000climo sensitivity experiments). Y.-N. K. performed the data
637 analyses and visualizations. Y.-N. K., F. L., C. D., I. R. S., S.-I. S., J. A. wrote and edited
638 the initial versions of the manuscript. All the authors participated in discussions on
639 interpreting the results and contributed to improving the paper.